# Parity Quantum Optimization: Encoding Constraints

Maike Drieb-Schön, <sup>1, 2, \*</sup> Younes Javanmard, <sup>1, \*</sup> Kilian Ender, <sup>1, 2</sup> and Wolfgang Lechner <sup>1, 2, †</sup>

<sup>1</sup>Parity Quantum Computing GmbH, A-6020 Innsbruck, Austria

<sup>2</sup>Institute for Theoretical Physics, University of Innsbruck, A-6020 Innsbruck, Austria

Constraints make hard optimization problems even harder to solve on quantum devices because they are implemented with large energy penalties and additional qubit overhead. The parity mapping, which has been introduced as an alternative to the spin encoding, translates the problem to a representation using only parity variables that encodes products of spin variables. In combining exchange interaction and single spin flip terms in the parity representation, constraints on sums and products of arbitrary k-body terms can be implemented without additional overhead in two-dimensional quantum systems.

### INTRODUCTION

Side conditions to optimization problems are crucial for many problems that are encountered in science, technology, and industry, ranging from scheduling problems to quantum chemistry [1–8]. Developing algorithms that solve these problems is notoriously harder compared to their unconstrained counterparts. Quantum computing as a new paradigm of computing that aims at enhancing optimization algorithms by making use of quantum phenomena may improve upon existing algorithms. However, quantum computers are limited in fidelity, control, and connectivity [9–14] which makes encoding of optimization problems one of the current grand challenges in the field. Side conditions are an additional complication to the encoding challenge. They are typically encoded via large energy penalties [15–17], which introduce an additional energy scale to the computation, making algorithms, such as QAOA or adiabatic quantum computing [18–20], less efficient.

In this paper, we present the encoding of optimization problems with additional side conditions (i.e. hard constraints) in analog [21–28] and digital [29–32] quantum computers using the parity quantum computing scheme [33–35]. For this purpose, we introduce a combination of exchange interactions and spin-flip terms. The parity transformation encodes optimization problems in a lattice gauge model with local 3-body and 4-body interactions on a square lattice. We introduce exchange terms that only act on qubits that are part of the side condition and spin-flip terms that act on the rest of the qubits. Using a compiler [34], qubits can be arranged on the square lattice with some flexibility. In particular, one can place qubits that are part of the constraint in close vicinity and thus allow for local hopping terms only.

We consider an optimization problem in the form of a general k-body Hamiltonian

$$H = \sum_{i} h_{i} s_{i} + \sum_{i < j} J_{ij} s_{i} s_{j} +$$

$$+ \sum_{i < j < k} M_{ijk} s_{i} s_{j} s_{k} + \sum_{i < j < k < l} R_{ijkl} s_{i} s_{j} s_{k} s_{l} + \dots,$$
(1)

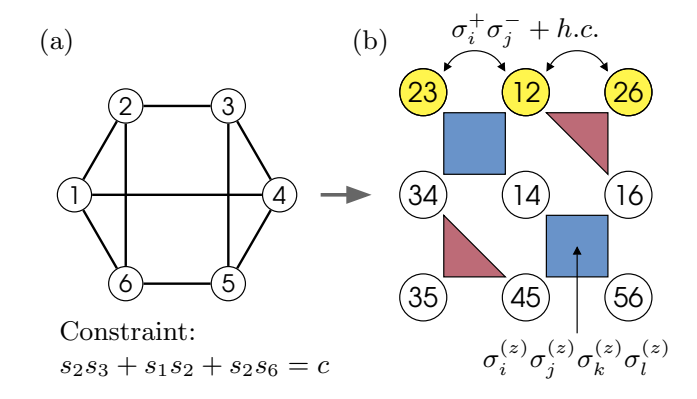


Figure 1. (a) The standard approach to encode optimization problems on a quantum device is to separate the unconstrained from the constrained part. The unconstrained part of the optimization problem is encoded as a spin model (top). Each node (circle) represents a logical spin, which can either be up or down. The edges (lines) represent interactions between the spins. The solution of the unconstrained part is the ground state of the spin model. In addition, a constraint on the spins is given (bottom). These constraints need to be implemented either by classical post-processing or additional large interactions. (b) In the parity encoding, the problem is translated to a Hamiltonian that encodes the unconstrained as well as the constrained part. The unconstrained part is encoded in a lattice gauge model, where nodes represent parity variables and interactions are local 3-body (red) or 4-body (blue) terms. The constraints are implemented as exchange terms among parity qubits that are part of the constraint term (yellow).

where  $s_i$  are the spin variables with values in  $\{-1,1\}$ . This Hamiltonian can be efficiently implemented using the parity transformation [34]. We assume that the terms can go up to N-body terms and the interaction matrices J, M and R are sparse. We assume the total number of qubits is N and the number of terms in the Hamiltonian is K.

In addition to the k-body optimization problem we consider a list of side conditions where each condition m can be written as

$$c_m = \sum s_i + \sum s_i s_j + \sum s_i s_j s_k + \dots \tag{2}$$

In this most general form, they contain sums and product terms, i.e. sums of single-body terms, 2-body terms, 3-body terms and so on.

The parity transformation [33] translates each term in the Hamiltonian in Eq. (2) to a single parity qubit. For a detailed explanation of the parity transformation see Ref. [34]. Here, we summarize the most important aspects for completeness: A parity qubit represents the product of spins in the z-basis, e.g.,  $\sigma_{123}^{(z)} = s_1 s_2 s_3$ . The parity transformation then describes the graph in terms of parity variables. This step increases the number of degrees of freedom from N to K, where N is the number of spins and K is the number of edges (or hyperedges). Thus, K - N + D parity constraints are introduced to restrict the low-energy subspace to the original size, where D is related to the degeneracy of the Hamiltonian (see [34]). The parity constraints are constructed from generalized closed loops in the logical graph e.g.  $\sigma_{12}^{(z)}\sigma_{26}^{(z)}\sigma_{16}^{(z)}$ is a valid parity constraint as the corresponding product in the logical variables is always +1. The main challenge in the parity transformation is to select K - N + D generalized closed loops such that the resulting parity constraints can be laid out on a chip in a local space-filling manner. For an all-to-all connected model, the choice of loops and the layout was shown in Ref. [33]. For arbitrary hypergraphs, the choice and arrangement of qubits is done compilation [34].

To avoid confusion between parity constraints and constraints of the optimization problem we will refer to the constraints of the optimization problem as side conditions. Side conditions of the form of products can be natively encoded in the parity mapping as shown in Ref. [34]. Side conditions on the sum of products, as in Eq. (2), are arbitrary sums and products (polynomials) of logical spins and will be discussed here.

In the state-of-the-art encoding of optimization problems, side conditions are imposed as large energy penalties. E.g., the side condition  $s_1s_2+s_2s_3=+1$  would be imposed by adding the energy term  $C(\sigma_1^{(z)}\sigma_2^{(z)}+\sigma_3^{(z)}\sigma_4^{(z)}-1)^2$  to the problem Hamiltonian. If C is large enough, the ground state of the Hamiltonian will satisfy the side condition. The challenges that come with this method are twofold: Firstly, the additional terms are higher-order (in the above example fourth order) which introduces an additional overhead when embedding it in physical hardware with pair interactions. Secondly, the constant C needs to be large, introducing an additional energy scale to the system, which is unfavorable for the implementation as well as for the dynamics.

Here, we present a different approach where side conditions are implemented in the dynamics rather than in the energy term i.e., by the driver Hamiltonian in the form of exchange terms [36, 37]. In combination with a compiler that is able to lay out qubits, these exchange terms are

only among nearest neighbors. Our strategy is to split up the parity qubits in two sets: 1.) qubits that are not part of the side condition terms, [U] and 2.) qubits that are part of the side condition terms [C]. Fig. 1 illustrates this setup for a particular example. In this example, the side condition include qubits 23, 12, and 26 which are in [C] (yellow) and the rest of the qubits are in [U] (white).

In this protocol, terms that are part of [U] are driven with single body  $\sigma^{(x)}$ , while terms in [C] are driven by exchange terms. These exchange terms (or hopping terms) between qubits in the set [C] are of the form  $\sigma_i^+\sigma_j^- + \sigma_i^-\sigma_j^+$ . The global ground state of this exchange term is in the zero magnetization sector. However, the magnetization sector required by a side condition is  $\sum_{i=1}^{n} \sigma_i^{(z)} = c$ . The exchange Hamiltonian preserves the magnetization required by the side condition during the annealing process. The final state is the lowest-energy state in the magnetization (symmetry) sector which fulfills the side condition - which may, or may not be the true ground state. The idea is to start in a configuration that satisfies the side condition and, as the exchange term conserves the sum, the state will stay in the side-condition-satisfying subspace, i.e. the subspace of H(t) that satisfies the side conditions. The parity constraints (i.e. 4-body or 3-body terms) act on all qubits, including [C] and [U], the hopping term only on qubits in [C] and the spin flip term  $\sigma^{(x)}$  only on qubits in [U].

In the following we will describe the protocols for Hamiltonian dynamics and digital quantum computing.

#### HAMILTONIAN DYNAMICS

The optimization problem with side conditions encoded as described above can be solved using an adiabatic quantum computing protocol. Our protocol introduces a few novelties compared to standard quantum annealing: 1.) The initial state is a classical state similar to reverse annealing protocols [38]. 2.) We introduce exchange terms acting on parts of the system and single spin flips acting on the rest. 3.) The final state may not be the ground state but a lowest-energy state in a different symmetry sector.

As in all adiabatic protocols, we start from a state which is prepared in the ground state of an initial Hamiltonian. In quantum annealing, this is the ground state of the driver Hamiltonian. Here, the initial Hamiltonian reads as follows:

$$H_{\text{init}} = \sum_{i}^{[U]} \varepsilon_i \sigma_i^{(z)} + \sum_{i}^{[C]} c_i \sigma_i^{(z)}.$$
 (3)

The sum [C] runs over all qubits that are included in the side condition and [U] runs over the rest of the qubits. The coefficients  $\varepsilon_i$  are chosen randomly from  $\{-1,1\}$ . The coefficients  $c_i$  are chosen such that the side conditions are satisfied, e.g. for a side condition with  $\sum_{i}^{[C]} \sigma_{i}^{z} = +c$ , the local fields are chosen to fulfill  $\sum_{i}^{[C]} c_{i} = -c$ . The optimization problem is encoded in the local field of the final Hamiltonian consisting of

$$H_{\text{final}} = \sum_{i}^{N} J_{i} \sigma_{i}^{(z)}.$$
 (4)

and

$$H_{\rm C} = \sum_{l}^{[P]} C_l \prod_{i_l}^{[P_l]} \sigma_{i_l}^{(z)}.$$
 (5)

Here, the sum [P] runs over all parity constraints  $P_l$  and the product  $[P_l]$  runs over all qubits in the parity constraint  $P_l$ . Note that the number of qubits in  $P_l$  is  $|[P_l]| = k$  for a k-body parity constraint. In Fig. 1, we have two 3-body and two 4-body parity constraints.

The driver Hamiltonian acts only on qubits associated with the side condition terms,

$$H_{\text{drive}} = \sum_{i}^{[U]} \sigma_i^{(x)}.$$
 (6)

In addition to the above terms, an exchange term is introduced among [C], that is,

$$H_{\text{exchange}} = c_e \sum_{\langle i,j \rangle}^{[C]^*} \sigma_i^+ \sigma_j^- + h.c.$$
 (7)

Here, the bracket []\* denotes a sum over all pairs  $\langle i,j \rangle$  of neighboured qubits connected via an exchange term in [C] e.g., in Fig. 1 the number of terms in the side condition is |[C]|=3 and the number of exchange terms  $|[C]^*|=2$  as there are two possible exchange moves that can be done with nearest neighbors.

The full time-dependent protocol reads

$$H(t) = A(t)H_{\text{init}} + B(t)H_{\text{drive}} + C(t)H_{\text{C}}$$

$$+D(t)H_{\text{final}} + E(t)H_{\text{exchange}}$$
(8)

Here, the functions A,B,C,D, and E are chosen as follows

j	initial	during	final
A	1	finite	0
В	0	finite	0
$\mathbf{C}$	0	finite	1
D	0	finite	1
$\mathbf{E}$	0	finite	0

#### **Numerical Simulations**

To interpret the results we have to distinguish between the ground state of the optimization problem Hamiltonian without side condition,  $H_{\text{problem}} = H_{\text{final}} + H_C$ ,

which we call unconditioned ground state  $\Psi_{gs}^{(u)}$  and the ground state of the optimization problem with side condition, i.e. the side-condition-satisfying ground states  $\Psi_{gs}^{(c)}$ . The state  $\Psi_{gs}^{(c)}$  is what we are seeking and corresponds to the lowest-lying eigenstate of  $H_{\text{problem}}$ , which satisfies the side conditions.

In the following, we will give an example for (i) the case  $\Psi_{gs}^{(u)} = \Psi_{gs}^{(c)}$  and (ii) the case  $\Psi_{gs}^{(u)} \neq \Psi_{gs}^{(c)}$ . In the latter case a crossing of the energy levels must occur. In the following we present the protocol of the annealing process, discuss diabatic transitions and consider  $\Psi_{gs}^{(c)}$  and/or  $\Psi_{gs}^{(u)}$  to be degenerate. We will also consider the role of the initial state discuss how the role of multiple side conditions.

The numerical results are presented for a random example where the unconditioned part is encoded in the parity model with 9 qubits, as shown in Fig. 1(b). For details of the annealing protocol of all examples, we refer to the appendix A. The random problem instance is encoded in the local fields  $J_i$  as the field vector

$$J = (0.8, 0.6, 1.0, 1.0, 0.7, 0.7, 0.1, 0.6, 0.8)^T.$$
 (9)

For better comprehensibility, the first ten eigenstates of this problem are explicitly written out in the appendix (B1). The components of the field vector and of the system states correspond to the qubits in Fig. 1 in the order from top to bottom and from left to right, i.e. as  $(23, 12, 26, 34, 14, 16, 35, 45, 56)^T$ . Independent of the initial state, as long as it satisfies the side condition  $c = \sum_{i}^{[C]} \sigma_{i}^{z}$ , the system always ends up in the conditioned ground state. Nevertheless, the instantaneous energy spectrum and the dynamics of the evolution of the system are affected by the choice of the initial state. Therefore, for some choices of initial states, multiple level crossings to instantaneous excited energy states and back to the instantaneous ground state of (8) are possible (even for  $\Psi_{qs}^{(u)} = \Psi_{qs}^{(c)}$ , further discussed in appendix B) while in other cases the system remains in the ground state during the whole annealing process, as in Fig. 2(a).

If  $\Psi_{gs}^{(u)} \neq \Psi_{gs}^{(c)}$ , the final state  $\Psi(t_f) = \Psi_{gs}^{(c)}$  is equal to the lowest-energy eigenstate that satisfies the side condition. Therefore, there must be a level crossing, such that system can end up in the lowest-energy state in the symmetry sector satisfying the side condition. We consider the same problem example, and choose the side conditions such that the solution to the problem without side condition is different to the one with side condition. In Fig. 2(b) we present a numerical example to demonstrate this.

Note, that the energy of the instantaneous system state crosses different energy levels of the spectrum of the time-dependent Hamiltonian (8). If the solution of the problem with side condition is the n-th excited eigenstate of the problem without side condition, the instantaneous

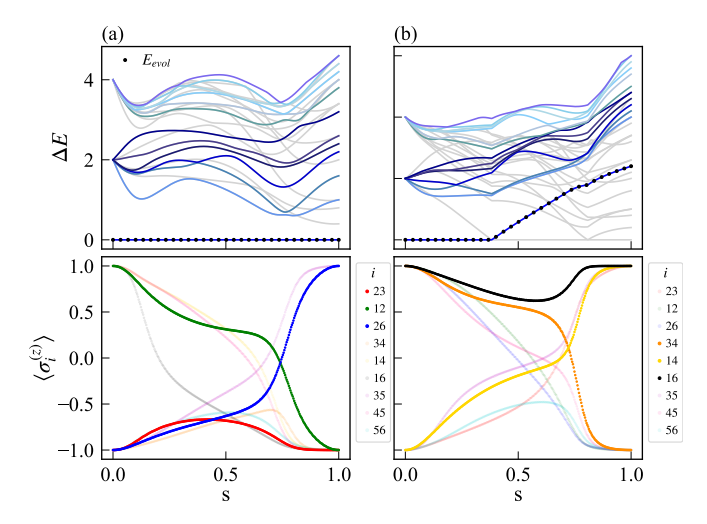


Figure 2. Adiabatic sweep for a system with N=9 qubits and time  $s(t) = t/t_f$  with  $t_f = 500$ . The top row in Fig. (a) and (b) shows the instantaneous energy spectrum, where all instantaneous eigenenergies of the time-dependent Hamiltonian in Eq. (8) are given with respect to the ground state energy,  $\Delta E = E_i - E_0$ . The energies of conditioned eigenstates, which lie in the side-condition-satisfying subspace are colored, while all the other ones are grey. The evolution of the system state energy  $E_{\text{evol}}$  (black dots) with time follows the instantaneous energy levels of the time-dependent Hamiltonian. The bottom row of Fig. (a) and (b) shows the time-dependent expectation value  $\langle \sigma_i^z(s) \rangle$  for each spin i, following the systems configuration state evolution in time. For the spins included in the side condition, the expectation values are highlighted, while the unconditioned ones are presented in pale colours. (a). The side condition is given by the sum constraint  $\sigma_{23}^{(z)} + \sigma_{12}^{(z)} + \sigma_{26}^{(z)} = -1$  and as the initial state we set  $\Psi_{(a)}(0) = |-1,1,-1,-1,1,1,-1,1,-1\rangle$ . The initial state and unconditioned ground state  $\Psi_{gs}^{(u)}$  satisfy the side condition. The energy of the system follows the instantaneous ground state energy. (b). For the side condition given by  $\sigma_{34}^{(z)} + \sigma_{14}^{(z)} + \sigma_{16}^{(z)} = 1$ , the conditioned ground state  $\Psi_{gs}^{(c)}$  is equal to the eighth excited state of the unconditioned problem. The initial state is set to  $\Psi_{(b)}(0) = [-1, 1, 1, 1, -1, 1, -1, 1, -1]$ , which satisfies the side condition. Therefore the energy of the time evolved system state crosses multiple energy levels of Hamiltonian in Eq. (8). The kinks in the energy spectra (as the one near s = 0.4 in (b)) occur because the energy difference to the instantaneous ground state is shown. They appear whenever the conditioned ground state energy leaves the instantaneous unconditioned ground state energy. Note that in the spectrum of the conditioned states (blue lines)  $\Delta E = E_i - E_0^{(c)}$ these kinks would vanish.

energy of the system has to cross at least n energy levels of the spectrum of the time-dependent Hamiltonian. This effect can be explained by the fact that the system is initialized in the instantaneous ground state and has to end up in an excited state after the adiabatic annealing process. If we only consider the subspace of side-condition-satisfying eigenstates (colored lines in bottom row of Fig. 2) we are able to see that the system follows

the instantaneous conditioned ground state without any level crossings inside this subspace.

Here the minimum energy gap between the conditioned ground state and the first excited state inside this subspace is crucial for the adiabatic condition [39] and gives a limit for the computation time  $t_f$ . In appendix C we discuss this in more detail and present an example for the adiabatic condition of the given annealing protocol.

In the case that the non-degenerate conditioned ground state is one of the degenerate ground states of the problem without side condition the unique solution is reached. For the case that the conditioned ground state  $\Psi_{gs}^{(c)}$  is degenerate the dynamics selects one of the states in the degenerate manifold. The precise form of the exchange Hamiltonian influences the probabilities with which the states are selected. Note, that a similar effect can be used to program superpositions in unconstrained models using the strength of the parity constraints  $C_l$  [40]. For more details of degenerate conditioned ground states we refer to the appendix (D).

Next we discuss multiple side conditions with different values  $c_j = \sum_i^{[C_j]} \sigma_i^{(z)}$  for j=1,...,M. If the different side conditions do not overlap, the method presented here can be trivially extended. If two side conditions overlap in one or more spins, this method with the given exchange Hamiltonian (7) cannot be applied directly. However, exchange terms are still useful if the overall sum of the spins included in the side conditions or, otherwise, if the sum of the overlapping spins for the conditioned ground state is known. We provide an example in the appendix (E).

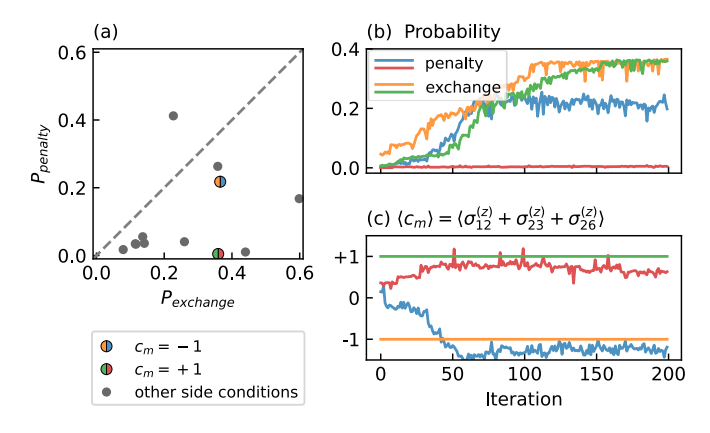
## DIGITAL QUANTUM COMPUTING

In digital quantum computing, an initial state is transferred to a final state via unitary operations. In the quantum approximate optimization algorithm (QAOA) [29] these unitaries are constructed from the Hamiltonian encoding the optimization problem and a driver Hamiltonian, usually given by single body  $\sigma^{(x)}$  terms. In our approach the unitaries are defined by their corresponding Hamiltonians from Eq.(8) which also includes exchange terms (Eq.(7)) as driver terms, for example

$$U_{\text{final}}(\alpha) = \exp(-i\alpha H_{\text{final}}).$$
 (10)

Each unitary contains a parameter (here  $\alpha$ ) which is variationally updated in the QAOA. To be able to reach every state fulfilling the side conditions, the exchange term cannot be directly translated to a unitary, but has to be applied in a staggered way, e.g.

$$U_{\text{exch.}}(\delta, \epsilon) = \exp(-i\delta(\sigma_j^+ \sigma_k^- + \sigma_j^- \sigma_k^+)) \times \exp(-i\epsilon(\sigma_k^+ \sigma_l^- + \sigma_k^- \sigma_l^+))$$
(11)



Comparison of the QAOA performance using exchange terms and energy penalties to treat side conditions. (a) Scatter plot of the maximum probabilities reached for a given selection of side conditions (see main text) for the exchange protocol against the penalty protocol. point  $(P_{\text{exchange}}, P_{\text{penalty}})$  represents the maximum probabilities reached for a specific target-state (given by the side condition and the value of c) for both protocols respectively. The side condition  $c_m = s_1 s_2 + s_2 s_3 + s_2 s_6$  is highlighted for  $c_m = -1$  (exchange/penalty in orange/blue) and  $c_m = +1$ (green/red). Panels (b) and (c) show the probability of measuring the target state and the expectation value of the sum of the qubits included in  $c_m$  during the QAOA protocol for the highlighted cases in panel (a). Note that in the exchange protocol  $\langle c_m \rangle$  is constant by definition, while the *penalty* protocol has an additional constraint to optimize.

for a side condition between qubits j, k and l. Applying the unitary corresponding to the complete side condition  $(\delta = \epsilon)$  would restrict one to reaching only states with symmetrically distributed excitations. The final state for a QAOA sequence of length p is then given by

$$|\psi\rangle = \prod_{j=1}^{p} U_{\text{exch.}}(\delta_j, \epsilon_j) U_{\text{drive}}(\gamma_j) U_{\text{C}}(\beta_j) U_{\text{final}}(\alpha_j) |\psi_0\rangle.$$
(12)

The initial state  $|\psi_0\rangle$  has to be prepared in the sidecondition-satisfying subspace, for example a specific computational basis state for the constrained qubits in [C], and the equal superposition of all basis states for the unconstrained qubits in [U]. Figure 3 shows a comparison of this approach (denoted exchange) with the fully parallelizable QAOA in the LHZ architecture introduced in [41] (denoted *penalty*), where each side condition is handled by adding an energy penalty to the cost function. We consider the optimization problem in Fig. 1(b) with the same local fields as in Eq.(9), and take into account all possible side conditions in either a row (e.g.  $s_1s_2 + s_2s_3 + s_2s_6$ ) or a column (e.g.  $s_2s_3 + s_3s_4 + s_3s_5$ ). For a fair comparison only the values  $c = \pm 1$  are chosen as side conditions, because for  $c=\pm 3$  the exchange term would have no effect on the state and would effectively reduce the problem size for the exchange protocol to 6 qubits. The state  $|\psi_0\rangle$  is initialized with the qubit in the first column (resp. row) of the side condition set to have  $\langle \sigma_i^{(z)} \rangle = -c$  and the others to c. The qubits in [U] are initialized in  $|+\rangle$ . The state for the *penalty* protocol is given by

$$|\psi\rangle = \prod_{j=1}^{p} U_{\text{drive}}(\gamma_j) U_{\text{C}}(\beta_j) U_{\text{final}}(\alpha_j) |+\rangle^{\otimes K}, \quad (13)$$

with the driver unitary treating all qubits as being in [U]. The cost function is given by  $E = H_C + H_{\text{final}}$ , with an energy penalty of the form

$$E_{\text{penalty}} = C \left( \sum_{i}^{[C]} \sigma_i^{(z)} - c \right)^2$$
 (14)

for the penalty protocol, where c denotes the value the side condition is restricted to.

The parameter updates in the classical optimization loop of the QAOA are done as follows: First we choose a random set of parameters and determine the value of the cost function E. At each iteration of the algorithm a randomly chosen parameter is updated by a random value in the interval [-0.1, 0.1]. If the cost function E decreases, the update is accepted. For the values shown in Fig. 3 this procedure is initialized 100 times with random parameters and the highest reached probability to find the target state is shown. To keep the number of parameters similar, p is set to p = 1 for the exchange protocol and to p=2 for the penalty protocol. The values of  $C_l$  in  $H_C$ and C in Eq.(14) are set to 4. The probabilities shown are defined as  $P = |\langle \psi | \psi_{\text{target}} \rangle|^2$ , where  $|\psi_{\text{target}} \rangle$  denotes the lowest-energy state fulfilling the side condition. We observe that both protocols perform comparably well if the ground state of the unconstrained problem also fulfills the side condition (the four points with  $P_{\text{penalty}} \geq 0.1$ in Fig. 3(a)). For the other cases the exchange protocol clearly outperforms the *penalty* protocol. In some cases (e.g. the red line in Fig. 3(b)) the penalty protocol does not converge to the true solution, even though the side condition is fulfilled. This might be remedied by directly including the energy penalty into the compilation process for the physical Hamiltonian (and thus also the QAOA unitaries), which in turn would require more hardware resources. In-depth benchmarking of the QAOA performance and its hardware requirements in these different approaches will be the topic of future research.

### CONCLUSION

We presented a method to implement and solve optimization problems with additional constraints in the parity architecture [33, 34]. We represent such constraints as driver terms in the form of an exchange Hamiltonian that keeps the system subspace that satisfies the side conditions. Our approach can be implemented in the current

quantum simulators and quantum computers based on two-dimensional arrays, including Rydberg atoms in optical lattices, ion surface chips, superconducting quantum computers, quantum dots, two-dimensional photonic systems, and NV centers, to name a few.

We compare the encoding of optimization problem in digital and analog applications and find a considerable improvement compared to standard encoding based on energy penalties. Note that in previous architectures, it has been shown that practically implementing such driver terms remains challenging [42, 43].

An interesting future outlook is to study the performance of encoded constraints in terms of driver Hamiltonian in the parity architecture in presence of noise or in finite temperature environment.

Acknowledgements - Work at the University of Innsbruck is supported by the European Union program Horizon 2020 under Grants Agreement No. 817482 (PASQuanS), and by the Austrian Science Fund (FWF) through a START grant under Project No. Y1067-N27 and the SFB BeyondC Project No. F7108-N38, the Hauser-Raspe foundation. This material is based upon work supported by the Defense Advanced Research Projects Agency (DARPA) under Contract No. HR001120C0068. Any opinions, findings and conclusions or recommendations expressed in this material are those of the author(s) and do not necessarily reflect the views of DARPA.

- \* authors contributed equally
- † wolfgang@parityqc.com wolfgang.lechner@uibk.ac.at
- [1] E. Farhi, J. Goldstone, S. Gutmann, J. Lapan, A. Lundgren, and D. Preda, Science **292**, 472 (2001).
- [2] D. Allouche, I. Andre, S. Barbe, J. Davies, S. de Givry, G. Katsirelos, B. O'Sullivan, S. Prestwich, T. Schiex, and S. Traore, Artificial Intelligence 212, 59 (2014).
- [3] S. Gravel and V. Elser, Phys. Rev. E 78, 036706 (2008).
- [4] F. Neukart, G. Compostella, C. Seidel, D. von Dollen, S. Yarkoni, and B. Parney, arXiv:1708.01625 [quant-ph] (2017).
- [5] E. G. Rieffel, D. Venturelli, B. O'Gorman, M. B. Do, E. M. Prystay, and V. N. Smelyanski, Quantum Information Processing 14 (2015).
- [6] E. Hebrard, E. O'Mahony, and B. O'Sullivan, in Integration of AI and OR Techniques in Constraint Programming for Combinatorial Optimization Problems, Lecture Notes in Computer Science, edited by A. Lodi, M. Milano, and P. Toth (Springer, Berlin, Heidelberg, 2010).
- [7] M. W. Johnson, M. H. S. Amin, S. Gildert, T. Lanting, F. Hamze, N. Dickson, R. Harris, A. J. Berkley, J. Johansson, P. Bunyk, E. M. Chapple, C. Enderud, J. P. Hilton, K. Karimi, E. Ladizinsky, N. Ladizinsky, T. Oh, I. Perminov, C. Rich, M. C. Thom, E. Tolkacheva, C. J. S. Truncik, S. Uchaikin, J. Wang, B. Wilson, and G. Rose, Nature 473 (2011).

- [8] P. Cao, Z. Fan, R. X. Gao, and J. Tang, arXiv:1706.03141 [cs] (2017).
- [9] F. Arute, K. Arya, R. Babbush, D. Bacon, J. C. Bardin, R. Barends, R. Biswas, S. Boixo, F. G. Brandao, D. A. Buell, et al., Nature 574, 505 (2019).
- [10] H. Bernien, S. Schwartz, A. Keesling, H. Levine, A. Omran, H. Pichler, S. Choi, A. S. Zibrov, M. Endres, M. Greiner, V. Vuletić, and M. D. Lukin, Nature 551, 579 EP (2017).
- [11] J. Koch, T. M. Yu, J. Gambetta, A. A. Houck, D. I. Schuster, J. Majer, A. Blais, M. H. Devoret, S. M. Girvin, and R. J. Schoelkopf, Phys. Rev. A 76, 042319 (2007).
- [12] M. Saffman, T. G. Walker, and K. Mølmer, Rev. Mod. Phys. 82, 2313 (2010).
- [13] L. Henriet, L. Beguin, A. Signoles, T. Lahaye, A. Browaeys, G.-O. Reymond, and C. Jurczak, Quantum 4 (2020).
- [14] I. Bloch, J. Dalibard, and W. Zwerger, Rev. Mod. Phys. 80, 885 (2008).
- [15] Z. Bian, F. Chudak, R. B. Israel, B. Lackey, W. G. Macready, and A. Roy, Frontiers in ICT 3 (2016).
- [16] A. Douglass, A. D. King, and J. Raymond, in *Theory and Applications of Satisfiability Testing SAT 2015*, Lecture Notes in Computer Science, edited by M. Heule and S. Weaver (Springer International Publishing, Cham, 2015).
- [17] A. Lucas, Frontiers in Physics 2 (2014).
- [18] T. Kadowaki and H. Nishimori, Phys. Rev. E 58, 5355 (1998).
- [19] A. Das and B. K. Chakrabarti, Rev. Mod. Phys. 80, 1061 (2008).
- [20] P. Hauke, H. G. Katzgraber, W. Lechner, H. Nishimori, and W. D. Oliver, Reports on Progress in Physics 83, 054401 (2020).
- [21] K. Ikeda, Y. Nakamura, and T. S. Humble, Scientific Reports 9, 12837 (2019).
- [22] H. Irie, G. Wongpaisarnsin, M. Terabe, A. Miki, and S. Taguchi, in *Quantum Technology and Optimization Problems*, Lecture Notes in Computer Science, edited by S. Feld and C. Linnhoff-Popien (Springer International Publishing, Cham, 2019) pp. 145–156.
- [23] T. Stollenwerk, B. O'Gorman, D. Venturelli, S. Mandra, O. Rodionova, H. Ng, B. Sridhar, E. G. Rieffel, and R. Biswas, IEEE Transactions on Intelligent Transportation Systems 21, 285 (2020).
- [24] I. Hen and A. P. Young, Phys. Rev. E 84, 061152 (2011).
- [25] H. K. Ng, B. Sridhar, and S. Grabbe, Journal of Aerospace Information Systems 11 (2014).
- [26] E. Rieffel, D. Venturelli, M. Do, I. Hen, and J. Frank, Proceedings of the AAAI Conference on Artificial Intelligence 28 (2014).
- [27] D. Venturelli, D. J. J. Marchand, and G. Rojo, arXiv:1506.08479 [quant-ph] (2016).
- [28] G. Rosenberg, P. Haghnegahdar, P. Goddard, P. Carr, K. Wu, and M. L. de Prado, IEEE Journal of Selected Topics in Signal Processing 10 (2016), 10.1109/JSTSP.2016.2574703, conference Name: IEEE Journal of Selected Topics in Signal Processing.
- [29] E. Farhi, J. Goldstone, and S. Gutmann, arXiv preprint arXiv:1411.4028 (2014).
- [30] Z. Wang, N. C. Rubin, J. M. Dominy, and E. G. Rieffel, Phys. Rev. A 101, 012320 (2020).
- [31] J. Cook, S. Eidenbenz, and A. Bärtschi, in 2020 IEEE International Conference on Quantum Computing and

Engineering (QCE) (2020) pp. 83-92.

- [32] S. Hadfield, Z. Wang, B. O'Gorman, E. G. Rieffel, D. Venturelli, and R. Biswas, Algorithms 12 (2019).
- [33] W. Lechner, P. Hauke, and P. Zoller, Sci. Adv. 1, 1500838 (2015).
- [34] K. Ender, R. ter Hoeven, B. E. Niehoff, M. Drieb-Schön, and W. Lechner, to be published (2021).
- [35] M. Fellner, K. Ender, R. ter Hoeven, and W. Lechner, to be published (2021).
- [36] I. Hen and F. M. Spedalieri, Phys. Rev. Applied 5, 034007 (2016).
- [37] I. Hen and M. S. Sarandy, Phys. Rev. A 93, 062312 (2016).
- [38] Y. Yamashiro, M. Ohkuwa, H. Nishimori, and D. A. Lidar, Phys. Rev. A 100, 052321 (2019).
- [39] M. H. S. Amin, Phys. Rev. Lett. 102, 220401 (2009).
- [40] L. M. Sieberer and W. Lechner, Phys. Rev. A 97, 052329 (2018).
- [41] W. Lechner, IEEE Transactions on Quantum Engineering 1, 1 (2020).
- [42] V. Choi, Quantum Information Processing 7, 193 (2008).
- [43] W. Vinci, T. Albash, G. Paz-Silva, I. Hen, and D. A. Lidar, Phys. Rev. A 92, 042310 (2015).

#### APPENDIX

## Appendix A: Annealing protocol

Here we give more details on the annealing protocol used in our numerical examples. The time dependent protocol used in the numerical examples is given by  $A(s) = (1-s)^2$ ,  $B(s) = E(s) = \Gamma s(1-s)$  and C(s) = D(s) = s where  $s = t/t_f \in [0,1]$  and  $t_f$  is the final annealing time of the annealing process. Therefore the time-dependent Hamiltonian (8) is given by

$$H(s) = (1 - s)^{2} H_{\text{init}}$$

$$+ \Gamma s (1 - s) (H_{\text{drive}} + H_{\text{exchange}}) \qquad (A1)$$

$$+ s (H_{\text{final}} + H_{\text{C}}).$$

The factor  $\Gamma$  has to be chosen suitably. If  $\Gamma$  is too small the energy gap between the conditioned ground state and the next higher conditioned state may close. This means that large annealing times are needed in order to stay in the conditioned ground state during the annealing process. A large  $\Gamma$  introduces a new energy scale and the advantage over the method using penalty terms vanishes.

Here we use  $\Gamma=4$  for all examples. The strength of the parity constraints is set to  $C_l=-4$  and the exchange term constant  $c_e=1/2$  for all examples.

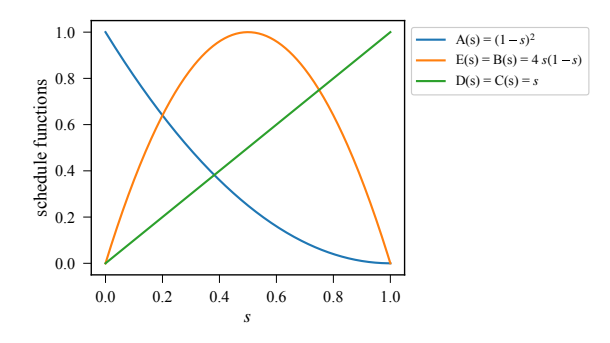


Figure 4. The annealing schedule used for the numerical examples in this work.

## Appendix B: Multiple level crossings

The combination of exchange terms and spin-flip terms may lead to multiple level crossings in the instantaneous energy spectrum even if the conditioned ground state is the ground state of the optimization problem without side conditions. We call it multiple level crossings, when the instantaneous conditioned ground state energy (lowest blue line in Fig. 5) crosses multiple instantaneous energy levels, which do not lie in the subspace of side-condition-satisfying states (grey lines in Fig. 5). Fig. 5 depicts the same random example as we used in the main text (9). Different initial states for different side conditions are used, which all are satisfied by

the unconditioned ground state, such that  $\Psi_{gs}^{(c)} = \Psi_{gs}^{(u)}$ . The first 10 eigenstates of the unconditioned problem Hamiltonian represented as spin configuration states  $|\psi_n\rangle = |n_{23} \ n_{12} \ n_{26} \ n_{34} \ n_{14} \ n_{16} \ n_{35} \ n_{45} \ n_{56}\rangle$  with  $n_i \in \{-1, 1\}$  are

with eigenenergies  $\varepsilon_0 = -4.1$ ,  $\varepsilon_1 = -3.7$ ,  $\varepsilon_2 = -3.3$ ,  $\varepsilon_3 = -3.1$ ,  $\varepsilon_4 = -3.1$ ,  $\varepsilon_5 = -2.5$ ,  $\varepsilon_6 = -2.1$ ,  $\varepsilon_7 = -1.9$ ,  $\varepsilon_8 = -1.7$ , and  $\varepsilon_9 = -1.5$ .

The exchange term enforces conservation of the sum of all spins included in the side condition, making the system stay in the subspace of side-condition-satisfied eigenstates during time-evolution. As the instantaneous ground state does not necessarily lie in this subspace, the multiple crossings of instantaneous energy levels can occur. This means that if we only consider the instantaneous spectrum of this subspace, we have an energy spectrum without any crossings between the conditioned ground state and the next excited state in this subspace.

# Appendix C: Adiabatic condition

Here we present an example for a non-adiabatic annealing process for the given annealing protocol (A1). Fig. 6 depicts a problem example with a small minimum energy gap between the conditioned ground state and the next higher conditioned state at  $s \simeq 0.8$  in the annealing process. We consider the minimum energy gap  $\Delta_{\min}$ in the subspace of the conditioned ground state and the next higher conditioned state. This can be understood from the instantaneous spectrum of the subspace, which is spanned by all eigenstates of (8) satisfying the side condition (colored lines in Fig. 6). We denote the energies of the subspace of side-condition-satisfying eigenstates as  $E_i^c(s)$ , while the energies of the full instantaneous spectrum are  $E_i$ . The conditioned ground state energy and the first excited conditioned state energy are given by  $E_0^c(s)$  and  $E_1^c(s)$  respectively. To estimate the computation time  $t_f$  for this annealing protocol we have to consider the minimum energy gap between  $E_0^c(s)$  and  $E_1^c(s)$ , i.e.  $\Delta_{\min} = \min_{0 \le s \le 1} E_1^c(s) - E_0^c(s)$ . This differs slightly from the annealing protocols where the minimum energy gap  $g_{\min} = \min_{0 \le s \le 1} E_1(s) - E_0(s)$  of the full instantaneous energy spectrum limits the process velocity.

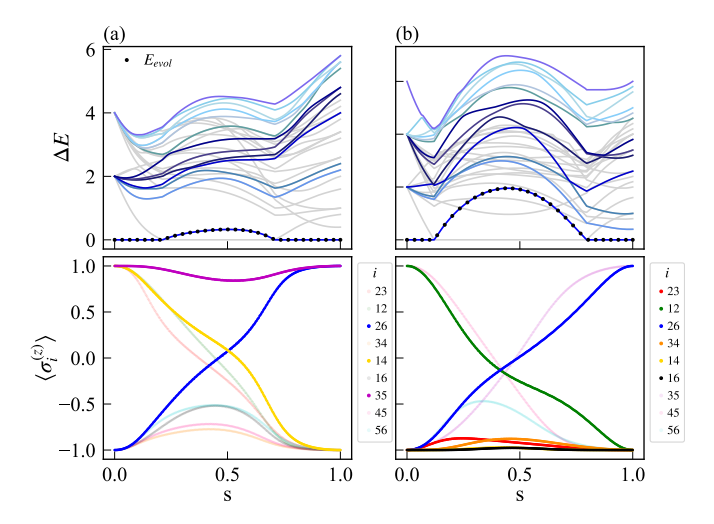


Figure 5. Adiabatic sweep for a system with N=9 qubits. The upper panel shows the instantaneous energy spectrum, where all instantaneous eigenenergies of the time-dependent Hamiltonian (8) are given with respect to the ground state energy,  $\Delta E = E_i - E_0$ . As in Fig. 2 the colored lines correspond to the energies of the subspace of eigenstates of (8) satisfying the side conditions. The kinks are level crossings between the energies  $E_0$  and  $E_1$  in the spectrum. At the level crossing two subspaces meet, that of the conditioned Hamiltonian and that of the full Hamiltonian. The Figures in the bottom row show the corresponding time-dependent expectation values of all spins  $\langle \sigma_i^z(t) \rangle$  for each site i of the system. (a). The side condition is given by the sum constraint  $1 = \sigma_{26}^{(z)} + \sigma_{14}^{(z)} + \sigma_{35}^{(z)}$  and the initial state is  $\Psi_{(a)} = |1 \ 1 \ -1 \ -1 \ 1 \ -1 \ 1 \ -1 \rangle$ . The initial state and the unconditioned ground state satisfy the side condition. The time evolution of the system state energy  $E_{\text{evol}}$  crosses the energy level of the first excited state and back to the ground state level. (b). The side condition is given by  $-4 = \sigma_{23}^{(z)} + \sigma_{12}^{(z)} + \sigma_{26}^{(z)} + \sigma_{34}^{(z)} + \sigma_{14}^{(z)} + \sigma_{16}^{(z)}$  and the initial state is  $\Psi_{(b)} = |-1\ 1\ -1\ -1\ -1\ -1\ -1\ -1\ -1\ )$ . The initial state and the unconditioned ground state satisfy the side condition. The time evolution of the system state energy  $E_{\text{evol}}$ crosses the energy level of the first up to the third excited state and back to the ground state level.

Here, zero energy gaps in the instantaneous energy spectrum during the annealing process are necessary to allow adiabatic level crossings.

By fine tuning the value of  $\Gamma$  and therefore increasing the minimum gap  $\Delta_{\min}$ , one can reduce the annealing time  $t_f$  required for adiabaticity. In Fig. 7 the same example as in Fig. 6 is given but for annealing processes with higher values for  $\Gamma$ . By increasing  $\Gamma$  we are able to shift the final annealing time to lower values. One can try to minimize computation times, by optimizing the value of  $\Gamma$ . But this has to be done carefully. If  $\Gamma$  becomes much larger (typically quadratically larger or more) compared to the energy scales of the system without  $H_{\text{exchange}}$ , it introduces a new energy scale. In practice this is critical with respect to the programmable interactions and can worsen error rates.

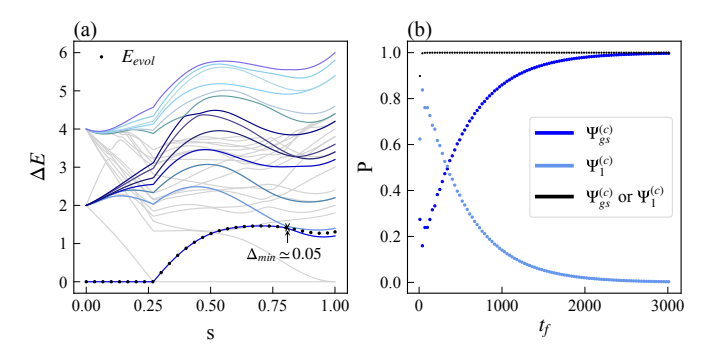


Figure 6. The colored lines are the energies of the instantaneous conditioned eigenstates of (8) (which satisfy the side condition) gapped to the instantaneous ground state energy  $E_0(s)$  of (8)  $\Delta E_i^c(s) = E_i^c(s) - E_0(s)$ . This Figure shows the instantaneous spectrum for a problem instance with a side condition that is satisfied by the second excited state (lowest blue line at  $t=t_f$ ), i.e. the conditioned ground state with  $E_0^c(s=1)=E_2(s=1)$ . The third excited state of the problem Hamiltonian also satisfies the side condition and is therefore the first excited conditioned state with  $E_1^c(s=1) = E_3(s=1)$ . Close to s=0.8 the annealing process becomes diabatic for  $t_f < 3000$ , because of the small minimum energy gap  $\Delta_{\min}$  between  $E_0^c(s)$  and  $E_1^c(s)$  at  $s \simeq 0.8$ . In this case the system ends up in a superposition of the conditioned ground state (second excited state) and the first excited conditioned state (third excited state). (a). Nonadiabatic sweep for  $s = t/t_f$  with  $t_f = 310$  and  $\Gamma = 4$ . The system leaves the adiabatic path and the process becomes non-adiabatic at the minimum energy gap  $\Delta_{\min}$  in the subspace of conditioned states (colored lines). (b). The probabilities P for the system to be in the conditioned ground state  $\Psi_{gs}^{(c)}$  ( $P = |\langle \Psi(t_f) | \Psi_{gs}^{(c)} \rangle|^2$ ) or in the first excited conditioned state ( $P = |\langle \Psi(t_f) | \Psi_1^{(c)} \rangle|^2$ ) in the subspace of of side condition satisfying states for different final annealing times  $0 < t \le 3010$ . For long enough annealing times  $(t_f > 3000)$ the system is in the conditioned ground state at the end of the annealing process.

## Appendix D: Degeneracy

Here we present an example to illustrate how the choice of exchange terms influences the probability distribution in a degenerate ground state manifold for the conditioned problem. We use a problem example encoded by the local field vector  $J = (1.0, -0.5, 1.0, -1.0, 0.5, -0.5, -1.0, -1.0, 1.0)^T$ . The first seven eigenstates of the unconditioned problem Hamiltonian represented as spin configuration sates  $|\psi_n\rangle = |n_0 \ n_1 \ n_2 \ n_3 \ n_4 \ n_5 \ n_6 \ n_7 \ n_8\rangle$  with  $n_i \in \{-1,1\}$  are

$$\begin{split} |\psi_0\rangle &= |-1 & 1 & 1 & 1 & -1 & 1 & 1 & 1 & -1 \\ |\psi_1\rangle &= | & 1 & -1 & -1 & 1 & 1 & 1 & -1 \\ |\psi_2\rangle &= |-1 & 1 & -1 & 1 & -1 & 1 & 1 & 1 \\ |\psi_3\rangle &= | & 1 & 1 & -1 & 1 & 1 & 1 & -1 \\ |\psi_4\rangle &= |-1 & 1 & -1 & 1 & 1 & 1 & 1 & 1 \\ |\psi_5\rangle &= |-1 & -1 & -1 & 1 & 1 & 1 & 1 \\ |\psi_6\rangle &= |-1 & 1 & -1 & 1 & -1 & 1 & 1 & 1 \\ \end{split}$$
 (D1)

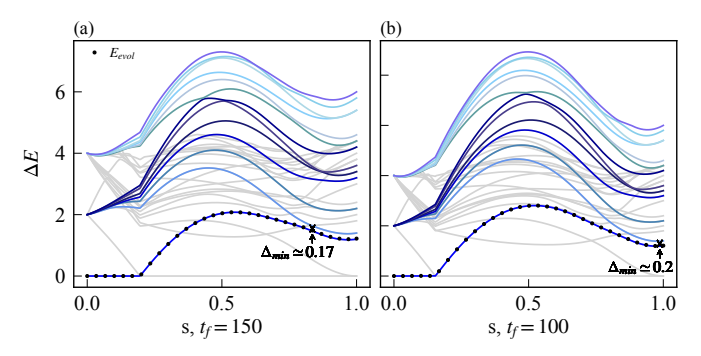


Figure 7. Instantaneous spectrum for the same example as given in Fig. 6(a) but for an annealing protocol with different values for  $\Gamma$ . (a).  $\Gamma=5$  and  $t_f=150$ . The minimum energy gap is increased to  $\Delta_{\min}\simeq 0.17$  at  $s\simeq 0.84$ . (b).  $\Gamma=6$  and  $t_f=100$ . The minimum energy gap is increased to  $\Delta_{\min}\simeq 0.2$  at  $s\simeq 0.99$ . For higher values of  $\Gamma$  the minimum energy gap does not increase much more and s goes to 1.

with eigenenergies  $\varepsilon_0 = -5.5$ ,  $\varepsilon_1 = -4.5$ ,  $\varepsilon_2 = -4.5$ ,  $\varepsilon_3 = -3.5$ ,  $\varepsilon_4 = -3.5$ ,  $\varepsilon_5 = -3.5$ , and  $\varepsilon_6 = -2.5$ . With the side condition  $-1 = \sigma_0^{(z)} + \sigma_2^{(z)} + \sigma_5^{(z)}$ , the conditioned ground state is three fold degenerate, because state  $|\psi_3\rangle$ ,  $|\psi_4\rangle$  and  $|\psi_5\rangle$  have the same energy and satisfy the side condition. We have four ways of constructing a valid exchange term  $H_{\text{exchange}}$  (7).

(i) 
$$\sigma_0^+ \sigma_2^- + \sigma_2^- \sigma_0^+ + \sigma_2^+ \sigma_5^- + \sigma_5^- \sigma_2^+$$

(ii) 
$$\sigma_0^+ \sigma_2^- + \sigma_0^- \sigma_2^+ + \sigma_0^+ \sigma_5^- + \sigma_0^- \sigma_5^+$$

(iii) 
$$\sigma_0^+ \sigma_5^- + \sigma_0^- \sigma_5^+ + \sigma_2^+ \sigma_5^- + \sigma_2^- \sigma_5^+$$

(iv) 
$$\sigma_0^+ \sigma_2^- + \sigma_0^- \sigma_2^+ + \sigma_2^+ \sigma_5^- + \sigma_2^- \sigma_5^+ + \sigma_0^+ \sigma_5^- + \sigma_0^- \sigma_5^+$$

We label the qubit sites independent of a distinct parity mapping and assume, that a compiler is able to lay out the qubits, such that each exchange Hamiltonian has only terms among nearest neighbors. For each of the four cases we let the system be in the same initial state  $|\psi_{\rm init}(0)\rangle = |-1,1,-1,-1,-1,1,-1,-1,-1\rangle$ . The results for this example are presented in Fig. 8. It demonstrates how the choice of the exchange term has influence on the distribution of the probabilities of the degenerate conditioned ground states. Further investigations are necessary to understand the influence of the exchange term onto the probability distribution.

# Appendix E: Overlapping side conditions

Here we consider the case of multiple side conditions in which some of them overlap in some of their spins. First let us consider multiple side conditions, which require different magnetic sectors

$$c_1 = \sum_{i}^{[C_1]} \sigma_i^{(z)}, ..., c_N = \sum_{i}^{[C_N]} \sigma_i^{(z)}$$
 (E1)

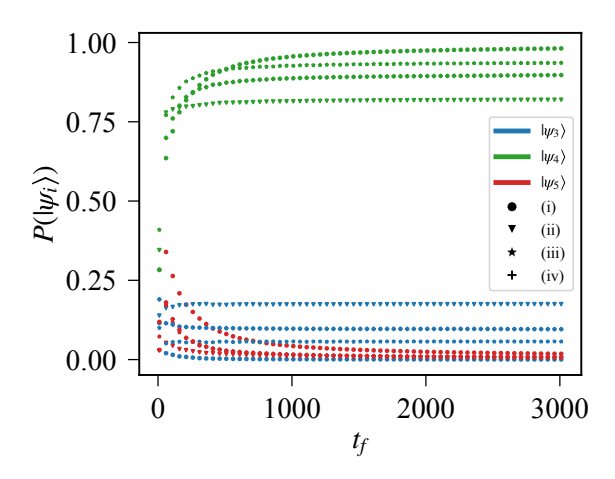


Figure 8. The probability  $P(|\psi_i\rangle) = |\langle \Psi(t_f)|\psi_i\rangle|^2$  to find the final system state in the state  $|\psi_i\rangle$  is given for the three degenerate ground states  $|\psi_3\rangle$ ,  $|\psi_4\rangle$  and  $|\psi_5\rangle$  (blue, green and red). It is calculated for final annealing times  $t_f$  between 0 and 3010 for each of the four valid exchange terms (four different markers). For the states  $|\psi_3\rangle$  and  $|\psi_4\rangle$  (blue and green) it is clearly visible that the choice of the exchange term changes their probabilities. For state  $|\psi_5\rangle$  (red) the difference in the probabilities is visible too, but weaker compared to the others.

For simplicity we consider the case with N=2 side conditions. The total set of spin indices in the system can be written as  $[U] \cup [C_1] \cup [C_2]$  and we define the set of indices of overlapping spins as the intersection  $[C_{\cap}] := [C_1] \cap [C_2]$  and the set of indices of both side con-

ditions together as  $[C_{\cup}] := [C_1] \cup [C_2]$ . If we introduce two exchange terms, one among  $C_1$  and the other among  $C_2$ , we can combine them to

$$H_{\text{exchange}} = c_e \sum_{\langle i,j \rangle}^{[C_1]} \left( \sigma_i^+ \sigma_j^- + \sigma_i^- \sigma_j^+ \right)$$

$$+ c_e \sum_{\langle i,j \rangle}^{[C_2]} \left( \sigma_i^+ \sigma_j^- + \sigma_i^- \sigma_j^+ \right)$$

$$= c_e \sum_{\langle i,j \rangle}^{[C_{\cup}]} \left( \sigma_i^+ \sigma_j^- + \sigma_i^- \sigma_j^+ \right) . \tag{E2}$$

This means, that the resulting exchange term conserves the total sum of all spins with indices in  $C_{\cup}$ . The conditioned ground state  $|\Psi_{gs}^{(c)}\rangle$  (i.e. the solution of problem with side conditions) is the eigenstate with lowest energy, which satisfies both side conditions simultaneously. Because the exchange Hamiltonian conserves the total sum of all spins in both side conditions combined, the final state does not necessarily have to be the correct solution of the problem with side conditions. In Fig. 9 we present a numerical example to demonstrate this problem. For the case of multiple side conditions with overlapping qubits we can not use this annealing protocol as presented here.

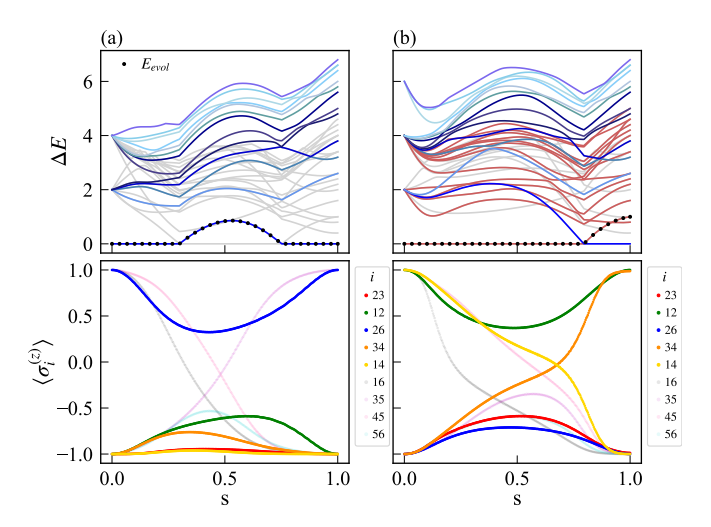


Figure 9. For the same problem instance as in the main text with the first ten eigenstates given by (B1), we are seeking for the eigenstate with lowest energy, which satisfies the two side conditions  $-1 = \sigma_{23}^{(z)} + \sigma_{12}^{(z)} + \sigma_{26}^{(z)}$  and  $-1 = \sigma_{26}^{(z)} + \sigma_{34}^{(z)} + \sigma_{14}^{(z)}$ . The two side conditions overlap in spin  $\sigma_{26}^{(z)}$ . The unconditioned ground state of the problem satisfies both side conditions and is therefore the conditioned ground state we are seeking for. (a). The initial state is given by  $|\Psi_{(a)}(0)\rangle = |-1 - 1 1 - 1 1 - 1 1 - 1 \rangle$ . The system state correspond to the solution of the conditioned problem in the end of the annealing process. (b). The initial state is given by  $|\Psi_{(b)}(0)\rangle = |-1\ 1\ -1\ -1\ 1\ -1\ 1\ -1\rangle$ and the system ends up in an excited state. If we compare it with the eigenstates in (B1) it is the third excited sate, which is the eigenstate which satisfies both side conditions and has  $\sigma_{26}^{(z)}=-1$  with lowest energy. While for the state  $|\Psi_{(a)}(0)\rangle$ the total sum of all conditioned spins is -2, for  $|\Psi_{(b)}(0)\rangle$  it is 0. So we can see that both lie in different subspaces of side conditions. The red lines in (b) show the energies of the subsystem of value 0, while the other colored lines are all of the subspace of value -2, in which the solution for the conditioned problem lies.